Focused fluid flow along faults in the Monterey Formation, coastal California

Peter Eichhubl*
James R. Boles
Department of Geological Sciences, University of California, Santa Barbara, California 93106, USA

ABSTRACT

Fluid flow in fractured siliceous mudstone of the Miocene Monterey Formation of California is inferred to be highly focused toward map-scale faults that locally contain extensive amounts of carbonate and minor silica cement. The distance of cross-stratigraphic flow, as inferred based on the strontium isotopic composition of carbonate fault cement, is close to the thickness of the Monterey Formation of 700 m in one of two study locations, Jalama Beach, and less than the formation thickness at another location, Arroyo Burro Beach. Fluid is thus derived from within the Monterey Formation rather than from underlying older units. Based on mass-balance estimates of the fluid volume required for fault cementation at Jalama Beach, the minimum distance of formation-parallel flow into the fault zone is 4 km and possibly >12 km. The inferred distance of flow parallel to the formation into this fault thus exceeds the distance of cross-formational upward flow along the fault by at least a factor of six. The mass-balance estimate requires that fluid flow along the fault is channeled into a pipe-shaped conduit rather than distributed along fault strike. Fluid flow from the surrounding formation into fault pipes is inferred to follow a radial rather than uni- or bilateral flow symmetry, using bedding-confined sets of extension fractures and stratabound breccia bodies. Radial fluid flow toward fault pipes requires fairly isotropic fracture permeability for flow along bedding and a low permeability across bedding. The inferred flow geometry illustrates the combined effect of fault permeability structure, permeability anisotropy of the surrounding formation, and hydraulic head distribution in controlling basinal fluid flow in faulted sequences.

Keywords: faults, fluids, strontium, isotopes, hydrocarbon, Monterey Formation.

INTRODUCTION

Faults may affect basinal fluid flow as barriers or as preferred conduits, depending on the difference in permeability between fault zone and the surrounding formation. Faults that are preferred conduits due to increased permeability parallel to the fault are likely to control the localized precipitation of pore cement and ore minerals and the migration and accumulation of hydrocarbons. Faults conducive for fluid flow can be subdivided into three hydraulic regimes (Fig. 1): (1) a source region where pore fluid is drawn into the fault zone from the surrounding formation of higher hydraulic head; (2) a sink region of lower hydraulic head where pore fluid is released back into the formation or onto the Earth's surface; and (3) an intermediate neutral conduit of no significant fluid exchange with the surrounding formation that may separate the source from the sink region. The effectiveness of fluid transport along a fault can be expressed as the total fluid volume that has migrated along the fault, the average flow rate, the distance of fault-parallel flow, and the distance perpendicular to the fault over which fluid is focused toward the fault in the source region and dispersed away from the fault in the sink region. An additional parameter of interest is the source volume, which is a function of fluid volume and source-rock porosity and storativity.

For the understanding of basinal hydrodynamics and associated transfer of mass and heat, it is of interest to quantify the extent to which conductive faults focus basinal fluid flow. In a sedimentary sequence undergoing dewatering and fluid expulsion during prograde burial and diagenesis, the extent of flow focusing by the presence of faults may be quantified by the ratio of fault-perpendicular flow distance over the distance of fault-parallel flow in the source region. In stratified sequences and for faults inclined with respect to the stratification, it may be more practical to consider the ratio between the distance of formation-parallel fluid flow ΔL over the distance of cross-stratigraphic flow ΔH within the source unit,

$$F = \frac{\Delta L}{\Delta H} \tag{1}$$

(Fig. 1). Fault systems with a large focusing ratio F will be more effective in channeling fluid expulsion from the source rock to a potential sink within the sequence or to the Earth's surface. However, in petroleum systems faults with large F will also be more effective for leaking hydrocarbons out of breached reservoirs.

For any fault of given length, the fluid focusing factor F is a function of the permeability anisotropy of the fluid source rock and of the distance to adjacent faults (Fig. 1). Large ratios of F would be expected in stratified source rocks with the highest permeability parallel to bedding, transected by faults of wide spacing. An isotropic permeability structure of the formation and/or close fault spacing would lead to low ratios of F. The permeability anisotropy of the source rock may be controlled by stratification within the formation (intrinsic anisotropy) and by the formation boundaries to overlying and underlying units (extrinsic anisotropy) (Fig. 1).

For a kilometer-scale fault system in the

*Present address: Department of Geological and Environmental Sciences, Stanford University, Stanford, California 94305, USA, and Monterey Bay Aquarium Research Institute, Moss Landing, California 95039, USA; e-mail: eichhubl@pangea.stanford.edu.

GSA Bulletin; November 2000; v. 112; no. 11; p. 1667–1679; 11 figures; 2 tables.

Monterey Formation in southern California, we demonstrate that the distance of formation-parallel fluid flow exceeds the distance of cross-stratigraphic flow by a factor $F \geq 6$. The distance of cross-stratigraphic fluid flow ΔH will be estimated using the strontium isotopic composition of carbonate fault cement as a natural tracer. The formation-parallel flow distance ΔL is inferred based on mass-balance estimates of the fluid volume that has migrated along the fault system. On the basis of the estimated distances of fluid flow and the characteristic permeability structure of Monterey rocks as observed in outcrop, we infer that the expulsion of basinal fluid in the Monterey Formation is highly focused toward faults by the intrinsic, layer-controlled permeability anisotropy of the formation (type A in Fig. 1).

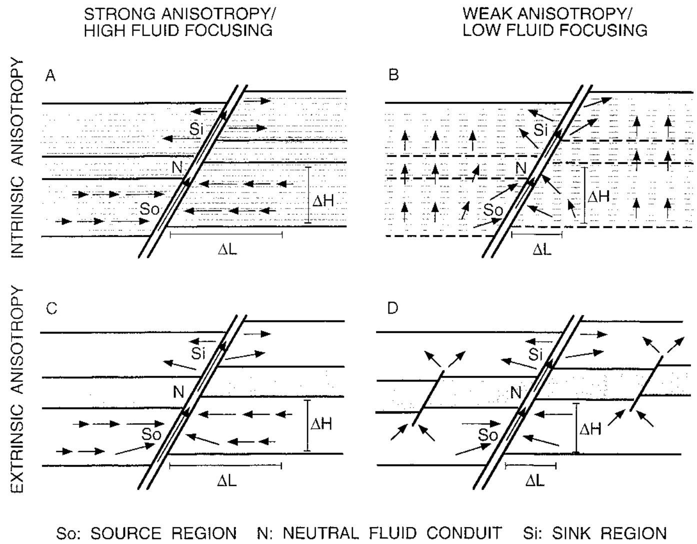

Figure 1. Geometry of upward-directed basinal fluid expulsion as controlled by faults and by the permeability anisotropy of sedimentary sequences. Conductive faults can be subdivided into source and sink regions and an intermediate neutral fluid conduit of no or minimal fluid exchange with the surrounding formation. The ratio of formation-parallel over cross-formational flow distance may be used to quantify the extent of fluid focusing toward faults in source units. Fluid focusing will be controlled by the permeability anisotropy of the source unit, which can be intrinsic, i.e., controlled by bedding, or extrinsic, i.e., controlled by contacts to overlying and underlying formations of low permeability. Fluid flow in the Monterey Formation is inferred to be strongly focused toward faults by the intrinsic anisotropy of the formation (case A).

STRUCTURAL SETTING OF CONDUCTIVE FAULTS

The Miocene Monterey Formation is an organic-rich, hemipelagic sequence of diatomaceous and phosphatic shale and organogenic dolostone, deposited between 18 and 6 Ma in a series of continental-borderland basins (Pisciotto and Garrison, 1981; Barron, 1986; Hornafius, 1994a). During burial, the organic-rich diatomaceous sequence underwent a complex sequence of diagenetic alteration, dominated by the following reactions: (1) silica transformation of diatom tests, from opal A via opal CT to quartz through two distinct steps of dissolution-reprecipitation (Stein and Kirkpatrick, 1976; Isaacs 1981); (2) degradation of organic matter and maturation of hydrocarbons (Petersen and Hickey, 1987; Baskin and Peters, 1992); (3) precipitation of authigenic dolomite during early diagenesis and subsequent dissolution and/or recrystallization (Burns and Baker, 1987; Compton, 1988; Malone et al., 1994); and (4) transition of smectite to illite (Pollastro, 1990; Compton, 1991). With an initial organic matter content of up to 34% (Isaacs and Petersen, 1987), the Monterey Formation is both source and reservoir rock for hydrocarbons (Ogle et al., 1987; MacKinnon, 1989). Due to the low matrix permeability, typically <1 md, hydrocarbon migration and production critically depend on fractures as flow pathways (Crain et al., 1985; Roehl and Weinbrandt, 1985; Isaacs and Petersen, 1987; MacKinnon, 1989).

Faults in the Monterey Formation are locally cemented by massive volumes of carbonate and quartz, indicative of large volumes of fluid flowing along these faults. At Jalama Beach, 100 km west of Santa Barbara (Fig. 2), two subparallel faults are cemented by dolo-

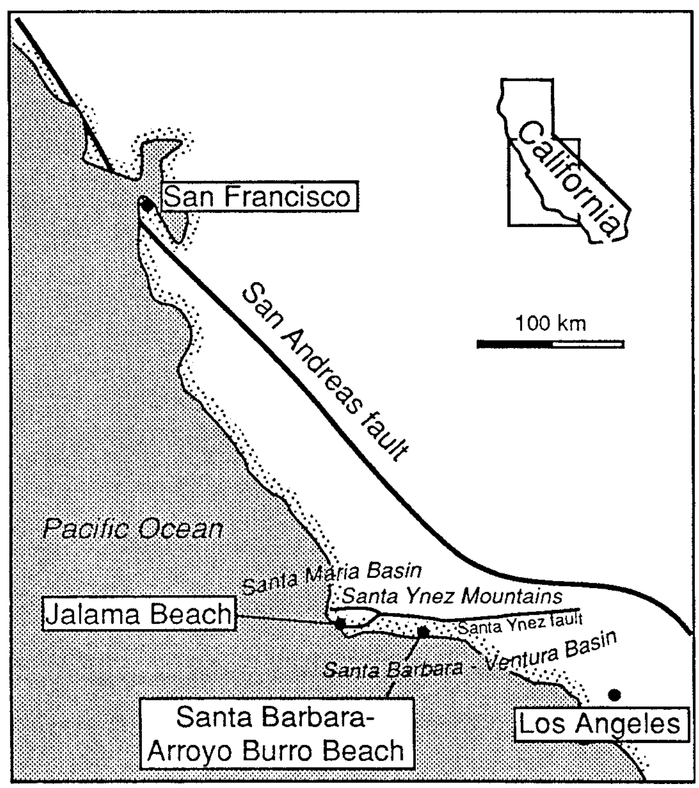

Figure 2. Location map of Jalama and Arroyo Burro Beaches in south-central California.

mite and minor amounts of quartz. The southern fault forms a resistant wall of cemented fault breccia, ~6 m thick, 7 m tall, and extending more than 35 m across the wavecut platform between mean low tide water line and the beach cliffs (Fig. 3). The second fault, ~300 m northwest of the first one, is less well exposed in a cove.

Both faults are characterized by a large amount of dolomite cement; 7–10-cm-thick layers of banded dolomite coat host rock fragments and aggregates of earlier dolomite cement (Fig. 3). Dolomite fault cement can be traced into extension veins that branch off from both faults and extend over distances of a few hundred meters (Fig. 4). The combined thickness of dolomite cement of both faults and connected veins, measured along a traverse across the strike of the fault-vein systems, is ~8 m. Fragments of cement and host rock fill interstitial cavities in fault cement. Sedimentary layering of infill and sorting of fragments by grain size suggest transport of detrital fracture fill in suspension by rapidly moving fluid along these faults (Eichhubl, 1997). The fault system at Jalama Beach is hosted by siliceous dolostone and dolomitic opal CT porcelanite and minor amounts of clay shale and chert.

A fault zone similar to that of Jalama Beach is exposed in coastal cliffs at Arroyo Burro Beach in Santa Barbara (Eichhubl and Behl, 1998). Two subparallel faults and associated veins are cemented by banded calcite of cumulative cement thickness similar to that of Jalama Beach. The host rock sequence at Arroyo Burro Beach consists of dolomitic porcelanite and siliceous mudstone and only subordinate dolostone.

Coastal sections of the Monterey Formation underwent for the most part a single burial-exhumation cycle; exhumation started ca. 1 Ma (Jackson and Yeats, 1982), while offshore sections of the Monterey Formation are still parts of active basins undergoing burial. The inferred maximum burial depth for the Jalama Beach section is ~1000 m (Eichhubl, 1997). The exposed fault system at Jalama Beach is ~50 m below the top of the Monterey Formation (Dibblee, 1988a, 1988b), which is ~700 m thick at this location (Grivetti, 1982). The fault system at Arroyo Burro Beach cuts across a bed of siliceous dolostone that marks the Luisian-Mohnian stage boundary (Echols, 1994; Hornafius, 1994c). On the basis of the measured thickness of the Naples Beach section (Echols, 1994; Hornafius, 1994c), located 22 km west of Arroyo Burro Beach, the fault system is ~300 m above the base of the Monterey Formation, which has a total thickness

Figure 3. Dolomite-cemented, left-lateral strike-slip fault at Jalama Beach. The southeastern one of two exposed faults (Fig. 4) extends for ~35 m across the wavecut platform. A former slip surface forms the margin of the fault zone to the right (northwest), and a second parallel slip surface is exposed on the left margin, to the left of the measuring stick (2 m long).

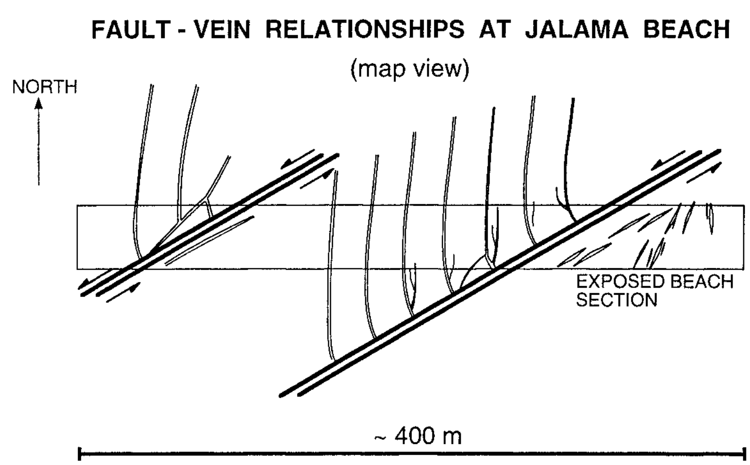

Figure 4. Map of cemented faults and associated vein systems at Jalama Beach, ~1.6 km northwest of state beach.

TABLE 1. $^{87}Sr/^{86}Sr$ COMPOSITION OF MONTEREY FAULT CEMENT

Sample number	Sample location	Description	$^{87}Sr/^{86}Sr$	$\pm 2\sigma$
03/01/95-7	Jalama Beach, southeastern fault zone	Early, randomly oriented dolomite cement	0.708820	0.000014
03/01/95-6AB	Jalama Beach, southeastern fault zone	Late banded, acicular dolomite	0.708815	0.000019
04/23/96-6	Jalama Beach, eastern margin of southeastern fault zone	Gray clear dolomite in fault-parallel vein	0.708874	0.000025
02/26/95-2	Jalama Beach, vein 145 m west of southeastern fault	Early banded clear dolomite, vein connected to fault (?)	0.708837	0.000014
02/26/95-2	Jalama Beach, vein 145 m west of southeastern fault	Late acicular dolomite, vein connected to fault (?)	0.708753	0.000014
02/11/95-5	Jalama Beach, veinlet 70 m east of southeastern fault	Isolated, bedding-confined dolomite veinlet	0.708829	0.000014
03/14/95-5A	Arroyo Burro Beach, eastern fault 600 m east State Beach	Early cement band of large calcite botryoid within fault	0.708765	0.000015
03/13/95-6	Arroyo Burro Beach, vein 20 m east eastern fault	Calcite vein, connected to fault	0.708749	0.000020
02/24/95-3B(B)	Arroyo Burro Beach, stratabound vein 88 m west aluminum tube, 1100 m east State Beach	Laminated calcite vein reactivating earlier dolomicrite vein across dolostone marker bed	0.708774	0.000025
04/25/94-5	Arroyo Burro Beach, stratabound breccia 4 m east aluminum tube, 1100 m east State Beach	Baroque dolomite cement in quartz-dolomite-calcite cemented dolostone breccia	0.708683	0.000014

Note: All $^{87}Sr/^{86}Sr$ values reported relative to NBS-987 standard = 0.710235. For detailed location description, refer to Eichhubl and Behl (1998). Sample numbers are same as used for stable isotopic analyses reported in Eichhubl and Boles (1998) and Eichhubl (1997).

of ~410 m at this location. The inferred maximum burial depth of the Arroyo Burro Beach section is 750 m (Eichhubl and Boles, 1998).

The faults and fault-related veins at Jalama and Arroyo Burro Beach dip steeply and cut across outcrop-scale folds, indicating fault and vein formation during shortening and exhumation of the basin flanks. The late, postfolding origin of these fault-related veins is also documented through untilted stratified detrital fracture fill. Abundant hydrocarbon fluid inclusions and bitumen-cemented breccias indicate that fault-related carbonate vein cementation is concurrent with hydrocarbon migration. Striations and drag of bedding indicate left-lateral strike slip for both fault systems. Displacements are estimated to be <100 m in both cases.

STRONTIUM ISOTOPIC COMPOSITION OF FAULT CARBONATE CEMENT AND HOST DOLOSTONE

The strontium isotopic compositions of carbonate vein and fault cement from Jalama Beach and Arroyo Burro Beach were analyzed in order to infer distances of mass transport. At Jalama Beach, microdrilled samples of banded, inclusion-poor dolomite cement from the eastern fault and from veins 145 m west and 70 m east of the eastern fault were analyzed. At Arroyo Burro Beach, calcite cement was sampled from the fault, from veins 20 and 400 m to the east, and from dolomite cementing a dolostone breccia 500 m east of the fault. In all cases, the composition and purity of carbonate cement were verified by thin-section petrography.

Carbonate samples were dissolved in 5 M acetic acid and the separated samples analyzed on a Finnigan MAT 261 adjustable five-collector mass spectrometer with a precision of <0.00003 (2σ mean; Table 1). The accuracy of the measurements was monitored with the NBS 987 standard, which gave a mean value of 0.710235 ± 0.00002 (2σ mean). Separations and analyses were performed in the laboratories of James Mattinson and George Tilton at the University of California, Santa Barbara.

In addition, four bulk rock samples of clay-poor, siliceous dolostone host rock were analyzed to provide a strontium-stratigraphic reference age of the section adjacent to the fault at Jalama Beach. Carbonate was dissolved using 5 M acetic acid to minimize contamination by clay dissolution and the $^{87}Sr/^{86}Sr$ ratio determined from the leachate (Table 2). Remaining carbonate in the dissolution residue was removed with 2.5 M hydrochloric acid until no visible reaction occurred. The acid was subsequently replaced two times to minimize strontium contamination in exchangeable clay layers, and the resulting HCl-insoluble residue was analyzed for $^{87}Sr/^{86}Sr$ (Table 2).

Strontium concentrations of the bulk rock and leachate obtained by X-ray fluorescence spectrometry (XRF) and thermal ionization mass spectrometry (TIMS), respectively, indicate that 5%–6% of total strontium of the bulk dolostone host rock from Jalama Beach is radiogenic strontium contained in clays. Following results by Schultz et al. (1989, Table 2), we assume that the radiogenic strontium resides in the nonexchangeable clay lay-

TABLE 2. ELEMENTAL AND STRONTIUM ISOTOPIC COMPOSITION OF SILICEOUS DOLOSTONE HOST ROCK AT JALAMA BEACH

Sample number	Location	SiO_2 (wt%)	CaO (wt%)	MgO (wt%)	Al_2O_3 (wt%)	K_2O (wt%)	Sr (ppm)	Rb (ppm)	HCl-insoluble residue (wt%)	Sr in residue (ppm)	Sr in residue (wt% of total Sr)*	$^{87}Sr/^{86}Sr$ of residue	Sr in carbonate† (ppm)*	Sr in carbonate† (wt% of* total Sr)*	$^{87}Sr/^{86}Sr$ of carbonate†	$^{87}Sr/^{86}Sr$ of bulk rock*
04/23/96-3	88 m west of southeastern fault	28.34	38.97	26.38	3.19	0.43	345	14	20	84.8	5.0	0.71104 ± 3	411	95.0	0.70895 ± 2	0.70905 ± 5
01/22/98-1	180 m west of southeastern fault§	51.86	26.35	13.68	1.97	0.39	300	13	39	43.6	5.7	0.71097 ± 3	464	4.3	0.70891 ± 1	0.70903 ± 4
04/23/96-8	80 m east of southeastern fault	41.89	31.83	18.70	2.93	0.55	244	19	35	44.3	6.3	0.71102 ± 2	351	93.7	0.70899 ± 2	0.70912 ± 4
01/22/98-3	110 m east of southeastern fault#	31.94	36.09	24.71	3.58	0.48	241	14	24	58.0	5.8	0.71160 ± 2	299	94.2	0.70886 ± 2	0.70902 ± 4

Note: All $^{87}Sr/^{86}Sr$ values reported relative to NBS-987 standard = 0.710235.
*Calculated value.
†Acetate leachate.
§Approximately 20 m stratigraphically below sample 04/23/96-3.
#15 m stratigraphically below sample 04/23/96-8.

ers that are largely unaffected by the acetic acid leach, whereas strontium in the exchangeable layers mimics the isotopic composition of the carbonate. This assumption is based on the similarity of our radiogenic strontium ratios of the dissolution residue with that of smectite in Schultz et al. (1989) after clay treatment with ammonium chloride, whereas the $^{87}Sr/^{86}Sr$ ratio of their untreated smectite samples compares to that of selectively leached carbonate pore cement. Negligible radiogenic strontium contamination during the selective acetic acid leach is also confirmed by the generally good correspondence of the strontium stratigraphic position of selectively leached carbonate samples with their biostratigraphic or lithostratigraphic position, as demonstrated by our samples and by Miller (1995), and as discussed in the following.

Strontium isotopic ratios for dolomite vein and fault cement at Jalama Beach, ranging between 0.70875 and 0.70887, are distinctly lower than dolomite (i.e., acetate leachate) values, 0.70886 to 0.70899, of surrounding host dolostone. Strontium isotopic ratios of calcite vein and fault cement at Arroyo Burro Beach are generally lower than vein and fault cement values from Jalama Beach, with values ranging between 0.70875 and 0.70877. The lowest $^{87}Sr/^{86}Sr$ ratio of 0.70868 is obtained from a single analysis of dolomite vein cement at Arroyo Burro Beach, 500 m east of the cemented fault. On the basis of crosscutting relations, this vein predates calcite fault and vein cement at Arroyo Burro Beach (Eichhubl and Boles, 1998).

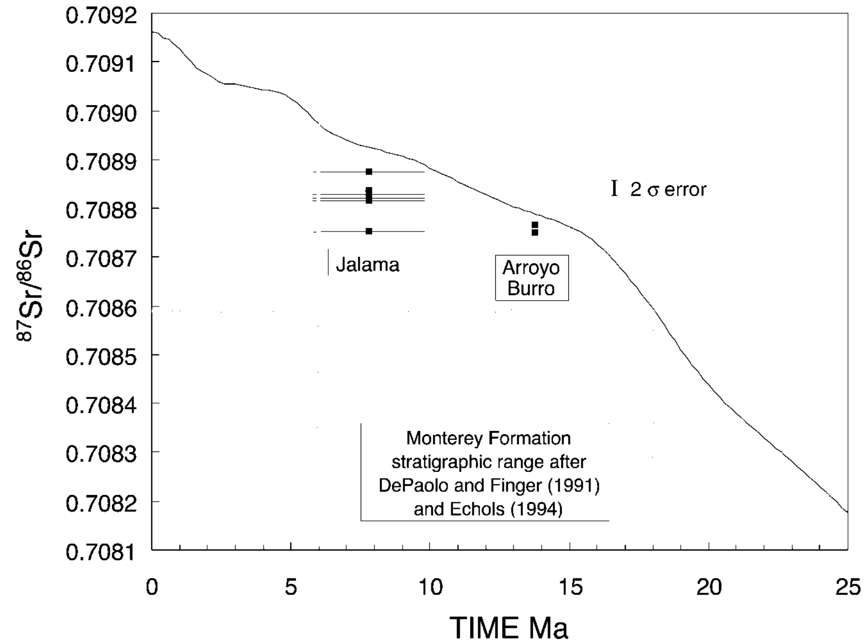

Figure 5. Strontium isotopic composition of Monterey vein carbonate. Strontium values are plotted with respect to the biostratigraphic age of the host rock (Arroyo Burro Beach) and with respect to the strontium isotopic composition of the host dolostone on both sides of the fault system (Jalama Beach). Horizontal bars on Jalama values represent the spread in strontium isotopic composition of the dolostone host rock. Seawater curve is after Howarth and McArthur (1997; revised second edition of database, written commun., August 1998). The 95% confidence interval of seawater curve is within line thickness. Time scale is after Shackleton et al. (1994) for 0–7 Ma and Cande and Kent (1995) for 7–25 Ma. Vertical error bar approximates 2σ standard deviation of vein cement analyses. All values are normalized to NBS 987 = 0.710235.

DISTANCE OF CROSS-STRATIGRAPHIC FLUID FLOW

For carbonate cement precipitating from an aqueous solution, the carbonate cement inherits the strontium isotopic composition of the aqueous solution, making the strontium isotopic composition of carbonate cement a useful natural tracer for basinal fluid flow (Schultz et al., 1989; Sullivan et al., 1990; Mountjoy et al., 1992; Chaudhuri and Clauer, 1993; Feldman et al., 1993). Throughout Neogene and Quaternary time the seawater $^{87}Sr/^{86}Sr$ composition steadily increased to the present-day value of 0.709162 (Howarth and McArthur, 1997) (Fig. 5). The strontium isotopic composition of entrapped pore fluid within a Neogene sediment sequence is therefore expected to decrease steadily with depth, provided the strontium isotopic composition of the fluid remained unmodified by diagenetic processes. Upward migration of pore water would lead to lower $^{87}Sr/^{86}Sr$ ratios in carbonate cement precipitating during or after fluid migration as compared to cement precipitated prior to fluid migration. The strontium isotopic composition of cement may thus be used as a tracer for cross-stratigraphic flow of connate pore fluids, provided that diagenetic changes in strontium isotopic fluid composition are negligible or predictable.

The strontium isotopic composition of the acetate-leached dolomite component in the four host dolostone samples from Jalama Beach agrees well with the upper Miocene stratigraphic position of the sampled section, ~50 m below the Monterey-Sisquoc contact as mapped by Dibblee (1988a, 1988b). Apparently, the selectively leached carbonate has retained the primary strontium isotopic composition of upper Miocene seawater. Similarly, Miller (1995) found a good correlation between strontium isotopic composition of acetic-acid leached dolostone and biostratigraphic age of samples taken from a continuous Monterey core from the South Elwood offshore oil field, 17 km west of Arroyo Burro Beach. Authigenic dolostone of the Monterey Formation has been shown to precipitate during early burial but is inferred to progressively recrystallize during burial, based on its oxygen isotopic composition (Burns and Baker, 1987; Malone et al., 1994). Miller's (1995) data indicate that, despite recrystallization, the dolostone beds remain closed with respect to strontium during recrystallization and oxygen isotopic resetting.

In contrast, the strontium isotopic values of calcite and dolomite vein and fault cement from Jalama Beach and Arroyo Burro Beach are distinctly lower than the expected seawater strontium isotopic values for the particular stratigraphic position of these locations (Fig. 5). For Jalama Beach, where a biostratigraphic reference is not available, $^{87}Sr/^{86}Sr$ ratios of fault and vein dolomite are compared to the measured $^{87}Sr/^{86}Sr$ composition of the surrounding host dolostone. For Arroyo Burro Beach, the $^{87}Sr/^{86}Sr$ composition of vein and fault cement is compared to the biostratigraphic age of the dolostone marker bed that corresponds to the Luisian-Mohnian stage boundary (Echols, 1994; Hornafius, 1994c) of ca. 13.85 Ma (Barron, 1986; time scale revised after Cande and Kent, 1995).

The average $^{87}Sr/^{86}Sr$ ratio of fault and vein dolomite at Jalama Beach of 0.70882 is 0.00011 lower than the mean $^{87}Sr/^{86}Sr$ value of the surrounding host dolostone (0.70893). For a formation thickness at Jalama Beach of ~700 m and assuming uniform sedimentation rate throughout the section, the difference suggests upward transport of strontium by ~245 m (±100 m for $^{87}Sr/^{86}Sr$ ratios ±0.00002 2σ). The inferred distance of upward strontium transport at Arroyo Burro Beach is less and close to the resolution limit of the method. Fault-related calcite cement at Arroyo Burro Beach has an average $^{87}Sr/^{86}Sr$ composition of 0.708757 ± 0.000020 that is 0.000031 ± 0.000023 below the expected value of 0.708788 ± 0.000003 for this particular stratigraphic position. For a thickness of the underlying Monterey section of ~300 m, this difference in isotopic composition is equivalent to 70 m (±50 m) of upward strontium transport. At both Jalama and Arroyo Burro Beach, the strontium isotopic composition of vein cement points toward a fluid source below the surrounding host rock but within the formation rather than within deeper sections of the basin.

The interpretation of these numbers as distance of upward fluid flow is contingent upon the following three assumptions.

1. The Strontium Isotopic Composition of the Pore Fluid has not Significantly Been Changed by Dissolution of Detrital Minerals

Mineral dissolution may change the strontium isotopic fluid composition. Dissolution of clays and potassium feldspar tends to increase the $^{87}Sr/^{86}Sr$ ratio, whereas dissolution of plagioclase tends to decrease the ratio of $^{87}Sr/^{86}Sr$. The extent to which these reactions alter the pore fluid strontium isotopic composition depends on the water-rock ratio, the strontium concentration in the mineral phase, and the mineral abundance. Potassium feldspar and plagioclase may contain 400–700 ppm Sr^{2+} (Schultz et al., 1989; Feldman et al., 1993), somewhat higher than Sr^{2+} concentrations in dolomite of 300–460 ppm measured at Jalama Beach (Table 2) and similar values reported previously (Faure, 1986; Burns et al., 1988). Potassium feldspar and calcic plagioclase form only a minor detrital component in Monterey rocks, of ~2% and 0.5%$_{weight}$, respectively (averages of 41 analyses; Compton, 1991). Volcanic ash beds, which occasionally contain Sr^{2+} in excess of 1000 ppm (Hornafius, 1994b), make up only ~1% of the total Monterey section and are therefore unlikely to affect the strontium isotopic composition of pore fluid on a regional scale. Carbonate, however, is abundant as authigenic dolomite and biogenic calcite (Isaacs, 1980; Burns and Baker, 1987; Compton, 1988).

Due to their higher abundance, clays have a potentially larger influence on the strontium isotopic composition of Monterey Formation water than feldspar. If we take (lacking a more systematic data set) the four host dolostone samples from Jalama Beach as a guide, complete dissolution of clay contained in these dolostones would raise the pore-water $^{87}Sr/^{86}Sr$ ratio by ~0.00013 as compared to pore fluid whose $^{87}Sr/^{86}Sr$ is controlled by carbonate dissolution only. Addition of radiogenic strontium would lead to an apparent decrease in inferred fluid migration distance. Assuming complete clay dissolution, addition of radiogenic strontium would thus double the migration distance of 245 m for Jalama Beach and quadruple the distance of 70 m for Arroyo Burro Beach. While the inferred fluid migration distances would be significantly longer, both estimates would still be within the thickness of the Monterey Formation at both locations, leaving the basic conclusion of an intraformational fluid source as derived earlier unchanged. Dissolution of smectite, the predominant clay phase in the Monterey Formation, has been observed at burial temperatures above 80 °C only (Pollastro, 1990; Compton, 1991). Thus, strontium release into the fluid due to clay dissolution is unlikely to be significant except within the deepest parts of the formation. The lack of a significant radiogenic strontium component in Monterey Formation water is also suggested by the strontium isotopic composition of present-day Monterey Formation water. Analyzed formation waters from three different Monterey reservoirs in the Santa Barbara and Santa Maria Basins, including the South Elwood offshore oil field studied by Miller (1995) with respect to dolomite strontium isotopes, range between 0.70863 and 0.70826 (Eichhubl, 1997), and are even lower than the strontium isotopic range predicted for connate Monterey Formation water based on the seawater curve.

Lacking any indication of a significant radiogenic strontium component in Monterey Formation fluids, the following discussion on fluid migration distance is based on the first estimates of 245 m for Jalama Beach and 70 m for Arroyo Burro Beach.

2. The Strontium Composition of the Fluid Corresponds to the Strontium Composition of a Distinct Source Layer

Equating the difference in strontium isotopic composition between the vein cement and some stratigraphic lower source layer with the distance of strontium transport is tantamount to assuming that all the strontium is derived from a single layer rather than from a depth range, and no exchange of strontium has taken place during upward flow. These assumptions are justified if a distinct stratigraphic horizon serves as an aquifer supplying fluid to the fault zone, and provided that carbonate dissolution or precipitation during upward flow does not cause significant exchange of strontium with the country rock. Because no single distinct aquifer can be identified in the sections at Jalama Beach and Arroyo Burro Beach, we assume that fluid is drawn into the fault uniformly from the underlying section over a finite depth interval and with uniform strontium concentration. Assuming a uniform strontium concentration of fluid entering the fault will be better justified by the uniformity of the dolostone-rich section at Jalama Beach (Grivetti, 1982) than for the more variable lithologic composition of the Arroyo Burro Beach section.

Assuming uniform fluid influx with uniform strontium concentration over the depth interval transected by the fault, the strontium isotopic composition of the fluid and thus of the cement at the top of the fault is the integrated strontium isotopic composition over the depth interval. If dissolved strontium enters the fault and fracture system over the depth interval h_{top}–h_{bottom} at equal amounts per unit depth interval Δh, then the strontium isotopic ratio of the fluid at the top of the depth interval is

$$^{87/86}Sr_{fluid} = \frac{1}{h_{top} - h_{bottom}} \int_{bottom}^{top} {}^{87/86}Sr_{formation}\, dh. \qquad (2)$$

In equation 2, $^{87/86}Sr$ stands for the strontium isotopic ratio and h_{top} and h_{bottom} correspond to the depth at top and bottom of the fault system, respectively. The isotopic composition of fluid entering the fault zone can be assumed to correspond to the strontium isotopic ratio of the formation at this particular depth h. With $^{87/86}Sr_{fluid}$ inferred through the measured isotopic composition of the vein cement and $d^{87/86}Sr_{formation}/dh$ approximated through the seawater strontium isotopic curve in Figure 5, equation 2 can be solved numerically to obtain h_{bottom}, the depth at the base of the depth interval drained by the fault system. The medium distance of mass transport thus obtained is 535 m (±120 m, ±2σ) for Jalama Beach and 140 m (±80 m, ±2σ) for Arroyo Burro Beach. For Jalama Beach in particular, and potentially for Arroyo Burro Beach, these distances are significant fractions of the thicknesses of the underlying formation, which is ~650 m at Jalama Beach (Fig. 6) and ~300 m at Arroyo Burro Beach. However, the inferred distances still do not suggest that strontium mass transport originates significantly below the base of the Monterey Formation.

Inferring $d^{87/86}Sr_{formation}/dh$ from the seawater strontium isotopic curve requires knowledge of variations in sedimentation rate within the particular stratigraphic interval. The transport distance obtained for Arroyo Burro Beach is corrected for sedimentation rates given by Echols (1994) for Naples Beach. For Jalama Beach, where a detailed biostratigraphic analysis is not available, we assumed a uniform sedimentation rate throughout the formation thickness. Because 535 m (±120 m) constitutes a large fraction of the total stratigraphic thickness of 700 m at Jalama Beach, variations in sedimentation rate throughout the section are likely to cancel out when integrated over the depth range.

If part of the strontium is continuously removed from solution by precipitation during upward flow in the fracture system, then the final strontium fluid composition in the fracture system can be estimated through the expression

$$^{87/86}Sr_{fluid} = \frac{\int_{bottom}^{top} {}^{87/86}Sr_{formation}(1 - \phi h)\, dh}{\int_{bottom}^{top} (1 - \phi h)\, dh}, \tag{3}$$

where ϕ is the fraction of strontium removed from solution through cement precipitation per unit flow distance.

The mass-balance calculation in the following section suggests that ~1.9×10^{-4} cm^3 dolomite per liter fluid per meter of flow distance precipitates during upward fluid flow. With an average concentration of 300 ppm Sr^{2+} in dolomite, cementation removes ~1.6×10^{-4} mg/L strontium per meter flow distance. Given an average strontium concentration of ~12 mg/L in Monterey Formation water (Eichhubl, 1997), the factor ϕ becomes ~1.3×10^{-5} m^{-1}. With the factor ϕ that small, the fluid strontium isotopic ratio obtained through equation 3 differs from that obtained through equation 2 by $<1 \times 10^{-6}$, which is within the precision of the strontium isotopic analyses—on average $\pm 2 \times 10^{-5}$ (2σ)—and therefore within the uncertainties of the distance estimates given herein.

As little as precipitation affects the estimates of mass transport distance, dissolution of host carbonate along the conduit wall will have an equally small effect on the strontium isotopic composition of the fluid. Fluid would have to enter and react with the host rock for tens to hundreds of meters adjacent to the fluid conduits for any significant shift in fluid strontium composition to occur. Host rock alteration visible in thin section, such as dolomite recrystallization, is restricted to within 1 m adjacent to fault-related veins at Jalama Beach. If dolomite recrystallization and accompanying strontium isotopic resetting of the host dolostone would have been more pervasive, the composition of the host rock samples on which the transport distance estimates are based would have been equally affected. Significant exchange in strontium isotopes between fluid and host rock during upward flow can thus be excluded.

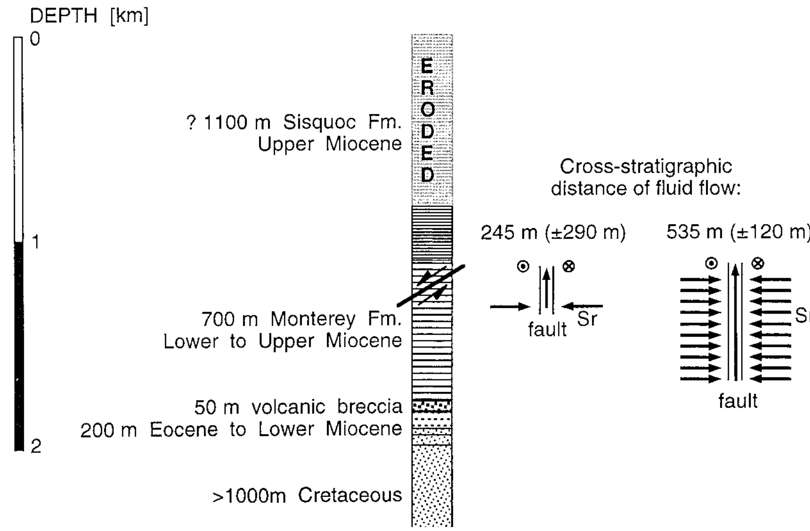

Figure 6. Inferred distances of cross-stratigraphic mass transport, based on the $^{87}Sr/^{86}Sr$ ratio of vein cement, plotted against the stratigraphic section at Jalama Beach. The lower estimate assumes a single source bed of fluid, and the higher estimate assumes that fluid is drawn into the fault uniformly over the depth interval. In both cases, a uniform sedimentation rate throughout the section is assumed, allowing substitution of the strontium isotopic sequence of the section by the $^{87}Sr/^{86}Sr$ seawater curve.

3. The Distance of Strontium Transport Corresponds to the Distance of Fluid Transport

The distances calculated herein refer to the transport of strontium, corresponding to distances of fluid flow only if strontium exchange between solution and country rock or earlier vein cement during upward flow is negligible. The calculation suggests that this is the case, the distances thus representing true distances of fluid flow. In sedimentary sequences, however, stratigraphic differences in $^{87}Sr/^{86}Sr$ composition reflecting the seawater strontium isotopic evolution during deposition will provide a proxy only for fluid flow across bedding, but not for bedding-parallel flow such as flow updip along the tilted flanks of the basin. The flow distance parallel to bedding is estimated in the following section based on a mass-balance calculation that estimates the fluid volume required for carbonate precipitation and by comparing the estimated fluid volume to a likely source volume.

VOLUME OF FLUID EXPELLED AND THE DISTANCE OF FORMATION-PARALLEL FLUID FLOW

The large volumes of carbonate cement contained in the fault zones at Jalama Beach and Arroyo Burro Beach are indicative of large fluid volumes and potentially effective focusing of fluid flow along these faults. In conjunction with the cross-stratigraphic flow distance derived herein, an estimate of the fluid volume necessary for precipitation of the observed volume of carbonate cement may provide an estimate of the distance of bedding-parallel flow and thus the extent of fluid focusing. The following discussion focuses on dolomite cementation at Jalama Beach but applies similarly to calcite cementation at Arroyo Burro Beach.

A mass-balance calculation of fluid involved in precipitation of the observed volume of dolomite requires information about the concentra-

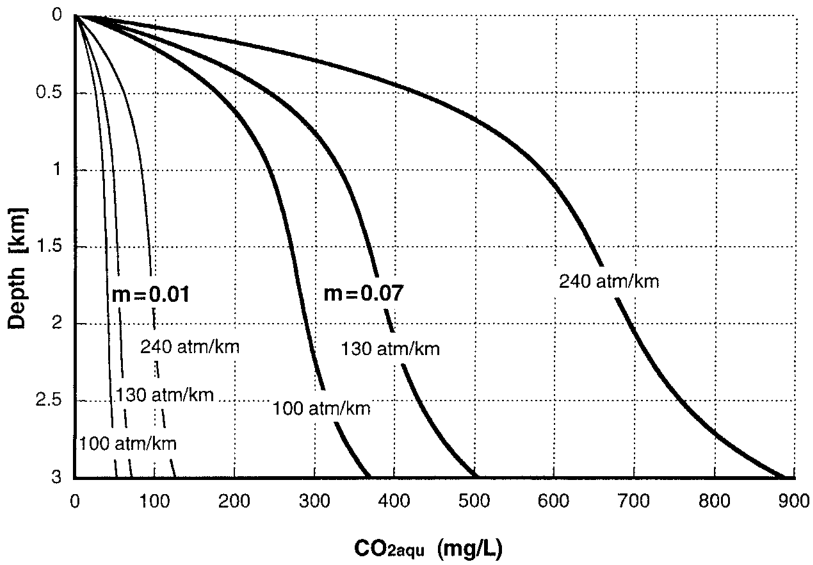

Figure 7. The variation of CO_{2aq} concentration in an aqueous solution as a function of depth and mole fraction m of CO_{2gas}. A CO_{2gas} mole fraction of 0.07 is measured in gas produced from the Hondo oil field (Exxon, Thousand Oaks, 1997, oral commun.), whereas a mole fraction of 0.01 is more characteristic for the temperature range of 80–100 °C (Smith and Ehrenberg, 1989). Curves are calculated for thermobaric gradients of 50 °C/100 atm (hydrostatic), 50 °C/240 atm (lithostatic), and 50 °C/130 atm, which is an upper limit of characteristic gradients in the Monterey Formation. The mole fraction of CO_{2aq} is calculated assuming a fugacity coefficient m = 1 and using Henry's Law coefficients after Ellis and Golding (1963) for 1 M NaCl solutions.

tions, or rather activities, of Ca^{2+}, Mg^{2+}, and CO_3^{2-}, and of pH, pressure, and temperature prior to and after upward fluid flow. Because these parameters are not known to the desirable extent, order of magnitude estimates need to be obtained by limiting the number of variables. The first estimate of fluid mass will be derived by assuming that cementation is controlled by the amount of Ca^{2+} and Mg^{2+} in solution. The second model assumes that Ca^{2+} and Mg^{2+} are not limiting factors, but that precipitation is controlled by changes in CO_2 partial pressure, other factors affecting pH being constant. In addition, reactions between a solid and an aqueous solution may not reach equilibrium if the solution is moving rapidly. A mass-balance calculation based on the assumption of thermodynamic equilibrium may thus provide only a minimum estimate of the mass of fluid involved. A third estimate is therefore obtained through observed precipitation rates in a moving solution under similar hydrodynamic conditions.

Cation-Limited Model

A conservative estimate can be obtained based on the assumption that dolomite precipitation is limited by the concentration of Ca^{2+} and Mg^{2+} in solution only, and that dissolved carbonate is available in excess. Concentrations of Ca^{2+} and Mg^{2+} in present-day Monterey Formation water in the Santa Barbara and Santa Maria basins average ~60 mg/L and 20 mg/L, respectively (Eichhubl, 1997). If all the magnesium were consumed to form dolomite, these concentrations correspond to a maximum of 153 mg or 0.05 cm^3 of dolomite per liter solution. The entire fault system, having a cumulative cement thickness of 8 m and an estimated depth, based on the strontium transport, of 500 m, would thus require 8×10^7 m^3 fluid per meter fault length. Assuming that the cemented zone extends 35 m along strike of the fault, a total volume of 2.8×10^9 m^3 or 2.8 km^3 fluid is required for dolomite precipitation.

Because only a fraction of Mg^{2+} is likely to be removed from solution during upward flow, this estimate is unrealistic. The pumping of formation water to the Earth's surface during oil production and before sampling may resemble upward fluid flow in fault zones. During pumping, the formation water decompresses, thus degasses CO_2, and possibly precipitates carbonate as scale in wells (Boles and Ramseyer, 1987). Ca^{2+} and Mg^{2+} concentrations are therefore likely to be higher in the subsurface than their values analyzed at the surface. The analyzed formation water composition may therefore be considered the final fluid composition after rapid upward flow rather than the initial composition before flow.

Carbonate-Limited Model

A more viable approach to carbonate mass balancing is based on the assumption that the formation fluid is always saturated in Ca^{2+} and/or Mg^{2+} with respect to calcite or dolomite and that precipitation is controlled by changes in CO_2 partial pressure as fluid moves upward and decompresses. Initial saturation with respect to dolomite or calcite appears reasonable for fluid that has been in contact with dolostone and calcite shell tests for several million years. In a pure H_2O-CO_3^{2-}-Me^{2+} system, carbonate cementation is controlled by changes in temperature and CO_2 partial pressure, with the tendency for carbonate dissolution with decreasing temperature under constant P_{CO_2}, but for precipitation with decreasing P_{CO_2} under constant temperature (Ellis, 1959). Under common geobaric gradients, the pressure effect outweighs the temperature effect and carbonate precipitates during upward flow, to the saturation concentration of available divalent metal cations, primarily Ca^{2+} and Mg^{2+}.

The CO_2 concentration in solution can be calculated using Henry's Law

$$K_h = \frac{f_{CO_2}}{x}, \tag{4}$$

where K_h is Henry's Law coefficient and x is mole fraction of CO_{2aq} in solution. Under dilute conditions, the fugacity, f_{CO_2}, approaches the partial pressure P_{CO_2}, which is equal to the total pressure times the mole fraction of CO_{2gas}. The change in CO_{2aq} concentration with depth is shown in Figure 7 for a constant mole fraction CO_{2gas} of 0.07, which is the mole fraction of CO_{2gas} in the gas phase produced from the Monterey Formation in the offshore Hondo oil field 40 km west of Santa Barbara (Exxon, Thousand Oaks, 1997, oral commun.). Henry's Law coefficients are taken from Ellis and Golding (1963) for an ionic strength of 1 m and gas activity coefficients have been approximated by unity.

Equilibrium concentrations of dissolved CO_{2aq} are calculated in Figure 7 for three thermobaric gradients, hydrostatic (50 °C/100 atm), lithostatic (50 °C/240 atm), and in between (50 °C/130 atm), the latter corresponding to a pressure gradient of 130 atm/km or 0.6 psi/ft (12.7 MPa/km). Pore-fluid pressure gradients in Monterey hydrocarbon reservoirs range between hydrostatic and 0.6 psi/ft (U.S. Geological Survey, 1983; Crain et al., 1985). Upward flow of 500 m to the depth of interest, ~1000 m, and following a hydrostatic pressure gradient, leads to a drop in CO_{2aq} concentration of ~30 mg/L, corresponding to ~0.02 cm^3/L of dolomite precipitation. If the fluid were initially at a fluid pressure corresponding to a pressure gradient of 130 atm/km and were to drop to a hydrostatic pressure, then CO_{2aq} concentration would drop by ~130 mg/L, precipitating ~0.10 cm^3/L dolomite.

With the latter number providing a minimum fluid volume, the entire fault system with a cumulative vein thickness of ~8 m and an estimated depth of 500 m requires a minimum of 4×10^7 m^3 of fluid per meter fault length. Assuming this fluid volume corresponds to 5% of the source rock volume, the fault would drain a rock volume of at least 0.8 km^3 per meter fault length. Because the faults at Jalama Beach are exposed only over a distance of ~35 m along strike, these numbers can be interpreted in two ways. If the cemented zone is only 35 m long, the required fluid volume is 1.2×10^9 m^3, corresponding to a source volume of ~23 km^3 and a distance of radial fluid flow into the fault of 4.3 km. If the fault cementation were continuous along strike, focusing fluid bilaterally over a 500-m-thick depth interval, then the fault would have to drain an 800-km-wide zone to each side of the fault, which is wider than the basin. Clearly, cementation along the fault must be discontinuous along strike and the fault focused fluid radially.

To see how sensitive the fluid volume estimate is to the assumed pressure gradient, we may assume that upward fluid flow followed a hydrostatic pressure gradient throughout. In this case, the total fluid volume required to precipitate an $8 \times 35 \times 500$ m^3 dolomite-cemented zone is ~6.3×10^9 m^3, four times more than obtained for the superhydrostatic case herein. The drainage radius becomes 9 km, twice the value, all other parameters being held constant.

A fluid pressure gradient close to hydrostatic is not very likely during fluid expulsion at Jalama Beach, however, because fluid migration with respect to the formation under hydrostatic conditions is possible only when the section compacts through the stagnant water column during burial. One of us (Eichhubl, 1997) derived flow velocities of as much as 0.1 m/s based on sedimentary structures of detrital fracture fill. These high flow velocities and the inferred timing of fluid flow during basin margin exhumation require above-hydrostatic fluid pressures to induce fluid flow, thus making fluid pressure conditions close to the hydrostatic gradient unlikely. Evidence for lithostatic fluid pressures, however, is not observed. Extensive bedding-parallel veins that would indicate lithostatic fluid pressures are not found in the Monterey Formation, with the exception of some water sills inferred to form during early burial based on crosscutting relations with folds and faults. On the basis of these constraints and present-day fluid pressure gradients, an initial fluid pressure corresponding to an intermediate fluid pressure gradient of 130 atm/km may be considered a reasonable estimate of the fluid pressure before upward fluid flow.

In addition to fluid pressure, fluid volume estimates depend critically on the CO_2 partial pressure, which is a function of the mole fraction CO_{2gas}. For a CO_{2gas} mole fraction of 0.01, a more common value for hydrocarbon reservoirs in the 80–100 °C temperature range than 0.07 used herein (Smith and Ehrenberg, 1989), the fluid volume becomes 10 km^3, and the radius of radial drainage becomes 11 km. The CO_{2gas} mole fraction typically increases in hydrocarbon reservoirs with increasing burial temperature and depth (Smith and Ehrenberg, 1989). Curves of dissolved CO_{2gas} plotted against burial depth would therefore have a lower slope than the curves plotted for constant mole fraction CO_{2gas}, as shown in Figure 7. During rapid upward flow along fractures in a formation of low matrix permeability, fluid may not exchange CO_2 easily with the formation water at shallower depth. The fluid may therefore be expected to follow the closed-system trajectories shown in Figure 7. Upward fluid flow through the matrix of permeable formations, however, may follow trajectories for a decreasing mole fraction CO_{2gas} and correspondingly precipitate more carbonate cement per unit fluid volume and flow distance than would be expected for rapid flow along faults.

These calculations were obtained assuming, for the sake of convenience, a pure H_2O-CO_3^{2-}-Me^{2+} system. Pore water of the Monterey Formation, however, is characterized by high concentrations of organic acid (S.G. Franks, 1996, written commun.). The dissociation of organic acids, such as the reaction $CH_3COOH \leftrightarrow CH_3COO^- + H^+$ for the acetate-acetic acid pair, may control pH in addition to P_{CO_2}. Solutions with acetate concentrations below ~0.06 M (~3600 mg/L) at 100 °C would still precipitate carbonate through CO_2 exsolution, although to a lesser extent than in a solution whose pH is solely controlled by the carbonate system (Lundegard and Land, 1989). At higher acetate concentrations, loss of CO_2 leads to carbonate dissolution rather than precipitation. Acetate concentrations of coastal Monterey Formation waters are generally below this threshold, with an average concentration of 2500 mg/L (S.G. Franks, 1996, written commun.). Temporary fluctuations in organic acid concentration above this threshold may lead to stages of carbonate dissolution intervening precipitation of vein cement. Stages of dissolution in fault carbonate cement were observed through cathodoluminescence at Jalama and Arroyo Burro Beach (Eichhubl, 1997). In any case, due to the presence of organic acid in Monterey Formation water, the fluid volume estimates and the inferred flow distances calculated here for systems free of organic acid must be considered minimum estimates.

Two further assumptions are the pressure profile over the vertical extent of the fault zone, and the ratio of expelled fluid to source rock volume. The preceding calculation assumes that the pressure and temperature drop is gradually distributed over 500 m. This assumption agrees with pore-pressure profiles with depth for the Monterey Formation (U.S. Geological Survey, 1983) that suggest a gradual pressure increase with depth. In addition, it is expected that, after initial rupture of a seal, the largest gradient in pore fluid pressure is presumably where the fluid leaves the formation and enters the fracture network. Following the assumption made earlier, that fluid seeps into the fault zone over its entire depth range, the fluid pressure drop would be equally distributed over the estimated flow distance thickness of the cemented zone, which is assumed to be 500 m.

It is difficult to assess the ratio of expelled fluid to the volume of the source rock. This ratio estimate is necessary to relate the calculated fluid volume to the flow distance. The expelled fluid volume may correspond to a change in pore volume during compaction. Because of the abundance of hydrocarbon inclusions in Jalama Beach vein cement, fluid flow along the fault is likely to be the consequence of hydrocarbon maturation in the adjacent synclines of the basin. Ungerer et al. (1983) estimated a 57% volume gain for type II kerogen during hydrocarbon maturation, allowing for selective escape of CO_2 and H_2S. For an initial average organic matter content of 8% of the rock volume (Isaacs and Petersen, 1984), the possible volume gain amounts to ~5% of the initial source rock volume. Because organic matter will be lost prior to the activity of the fault system, 5% yield may be considered a maximum estimate, also leading to a minimum estimate in flow distance.

Kinetic Model

The preceding approach is based on the assumption that fluid is in thermodynamic equilibrium with wall-rock carbonate prior to and during flow. While this assumption is justifiable as an initial condition with a long residence time prior to fluid expulsion, sluggish reaction kinetics may prevent the solution from reaching equilibrium during upward flow. Long-term average flow velocities for Jalama Beach are ~1 m/day, based on inferred rates of heat loss during upward flow (Eichhubl, 1987).

Experimental kinetic data for dolomite precipitation at the temperatures of interest are not available. A crude estimate of the fluid volume required for precipitation of dolomite cement at Jalama Beach can be obtained, however, from the observed rate of calcite scale formation in well casings. Boles and Ramseyer (1987) reported calcite scale with a cross-sectional area of 21 cm^2 being precipitated from 89.1×10^3 m^3 of fluid over 3342 days (~9 yr) of hydrocarbon production at a depth of 2591 m in a Miocene sandstone reservoir. Precipitation is accompanied by a pressure drop from 4900 psi (33.8 MPa) to 400 psi (2.8 MPa) and degassing of the fluid. Mole percent CO_{2gas} averaged 1.7% over this period, increasing from ~0.13% to 2.16% (data by Arco, Bakersfield, provided to J.R. Boles, 1993).

Under the same conditions, 280 m^2 of calcite, equivalent to the surface area of dolomite at Jalama Beach, would require 12×10^9 m^3 or 12 km^3 of fluid, which is one order of magnitude higher than the best equilibrium estimate given herein. The corresponding radius of fluid drainage is 12 km. Although the reaction kinetics may be slower for dolomite, this estimate is based, in contrast to the equilibrium thermodynamic calculation here, on actual precipitation rates in a moving fluid. The average calculated flow velocity in the well casing is 0.3 L/s or ~20 cm/s.

DISCUSSION

The estimated distances of fluid flow, to 650 m across bedding and a minimum of 4–12 km parallel to the formation, is equivalent to fluid focusing by a factor $F \geq 6$ as defined in equation 1. This high degree of lateral fluid focusing indicates that the permeability of the formation away from faults is highly anisotropic, the highest permeability being parallel to bedding.

Fluid flow may preferentially follow bedding due to the following types of permeability anisotropy.

1. Bedding-parallel fluid flow may be channeled along beds of high matrix permeability that alternate with beds of low permeability, as in an alternating sequence of sandstone and shale. Rock types of the Monterey Formation are characterized by equally low matrix permeability (Crain et al., 1985; Roehl and Weinbrandt, 1985; Isaacs and Petersen, 1987; MacKinnon, 1989), with the exception of some dolostone beds that contain appreciable secondary porosity we observed in core from the offshore Hondo oil field. Dolostone from Jalama and Arroyo Burro Beach, however, appears to be tightly cemented throughout.

2. Fluid flow may follow partings parallel to bedding planes. Although siliceous rock types of the Monterey Formation typically part parallel to bedding in outcrop, it is not certain if bedding-parallel fractures are conductive for fluid flow in the subsurface. Mineralization along bedding planes is infrequent and, where cross-cutting relations are observed, appears to predate folding (Bartlett, 1994).

3. Fluid flow may follow bedding-confined fractures. Extension fractures oriented at high angles to bedding and confined to the more competent units of porcelanite and dolostone in sequences alternating with clay shale of low competence are characteristic of the Monterey Formation (Narr, 1991; Hickman and Dunham, 1992; Gross, 1995; Gross et al., 1998). Hydrocarbon fill and carbonate and silica cementation of these bedding-confined veins indicate that they serve as fluid pathways in the subsurface. Frequently, extension fractures in the more competent beds lead into normal faults in the overlying and underlying mudstone beds (Figs. 8 and 9). The connected system of normal faults and extension fractures was termed fault-fracture mesh by Sibson (1996), following Hill (1977). Fluid flow is likely to occur preferentially along the extension fractures, parallel to the bedding. Slip along the normal faults would lead to continued opening of the extension veins, possibly preventing complete sealing of extension veins by cementation. The permeability and connectivity of bedding-confined fractures may also be enhanced due to shear reactivation of fractures initially formed in extension (Dholakia et al., 1998).

4. Potential pathways for preferred fluid flow parallel to bedding are bedding-parallel breccia zones (Redwine, 1981; Roehl, 1981; Belfield et

Figure 8. Fault-fracture mesh in alternating sequence of opal CT porcelanite and organic-rich, phosphatic opal A mudstone at Arroyo Burro Beach. Porcelanite fails brittlely by forming extension fractures. Extension is accommodated in overlying and underlying mudstone by normal faults.

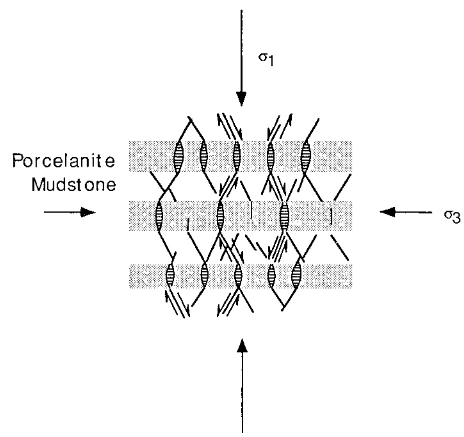

Figure 9. Schematic view of fault-fracture mesh, modified after Eichhubl and Behl (1998) and inspired by Sibson (1996) and Gross (1995).

Figure 10. Brittlely folded chert bed forming bedding-parallel breccia body. Hydrocarbon matrix of chert breccia indicates that breccia serves as fluid migration pathway. Photograph courtesy of Richard Behl, California State University, Long Beach.

al., 1983). Dholakia et al. (1998) documented the formation of bedding-parallel brecciation in the Monterey Formation due to differential slip between bedding planes, presumably caused by flexural slip in folds. Prominent breccia bodies in excess of 1 m thickness are also observed as the consequence of brittle folding of chert layers (Snyder et al., 1983; Hickman and Dunham, 1992; Behl and Garrison, 1994) (Fig. 10). Typically, diatomite and porcelanite layers overlying and underlying folded chert beds are unfolded, giving chert folds the resemblance of synsedimentary folds. Behl and Garrison (1994) suggested that brittle chert folds are tectonic, with the shortening accommodated in the overlying and underlying diatomite and porcelanite layers by bulk shortening and porosity collapse, whereas low-porosity chert buckles, brecciates, and folds. Brecciated chert layers are frequently found saturated with hydrocarbons.

The observed control of bedding on the fracture permeability structure suggests that the inferred permeability anisotropy of the formation and resulting fluid focusing are intrinsic to the formation (Fig. 1A) rather than controlled by formation boundaries (Fig. 1C). However, the degree to which the permeability anisotropy is intrinsic may vary on a regional scale and with depth. Porcelanite and chert in the quartz diagenetic stage may be sufficiently fractured to allow flow across bedding. The permeability anisotropy of the formation may then be controlled by diagenetic boundaries and by variations in silica and clay content of the formation with depth on the scale of stratigraphic members of the formation.

The mass-balance estimates require that fluid enters the faults in a radial rather than uni- or bilateral symmetry. It follows that faults are preferred pathways over short segments, forming pipes rather than planar ducts within these fault zones (Fig. 11). Possible pathways for fluid flow are releasing bends, extensional stepovers of fault segments, and fault intersections. Radial flow into these fluid pathways requires that fluid flow along bedding is fairly isotropic within the bedding plane. A single dominant joint set would likely result in a strong flow anisotropy within bedding planes (Fig. 11B). Radial and thus isotropic flow requires at least two or more crosscutting and mutually connected joint sets (Fig. 11C), as described by Gross (1993) from the Monterey Formation. Isotropic flow along bedding may be best accommodated by bedding-parallel breccia zones. Belfield et al. (1983) and MacKinnon (1989) reported that oil production is most prolific from wells intersecting the regional, north-northeast–south-southwest–trending joint set at high angles, a finding not supported by others (Jon Schwalbach, Exxon, Thousand Oaks, 1996, oral commun.) and inconsistent with the radial flow geometry inferred from this study. This ambivalence may indicate a regional variability in the permeability anisotropy for flow parallel to bedding.

Within the tilted sequence on the basin flanks, fluid will be drawn preferentially from the center of the basin or from adjacent synforms. This semicircle or arc of a circle geometry will extend the minimum distances of formation-parallel flow of 4 to >12 km by at least a factor of 2. An updip migration path of hydrocarbons from synforms undergoing burial and catagenesis into uplifted structural highs was also inferred by Ogle et al. (1987) based on the charge history of Monterey reservoirs.

The effect of faults on basinal fluid migration is thus governed by three geometric constraints: (1) the permeability structure of the fault zone such as the presence of zones of local extension along the fault; (2) the permeability anisotropy of the surrounding formation as controlled by stratification, jointing, and lateral stratigraphic variations; and (3) the orientation of the regional flow field as controlled by differences in hydraulic head. An analysis of all three components is required for the prediction of basinal fluid flow in faulted sequences, as done routinely by numerical modeling. Although the combination of low matrix and high fracture permeability is unique to the siliceous shale of the Monterey Formation, bedding or layering, lateral stratigraphic variations, and the preferred orientation of regional joint sets will create a permeability anisotropy in most sedimentary sequences as well as in basement rocks, thus affecting local-

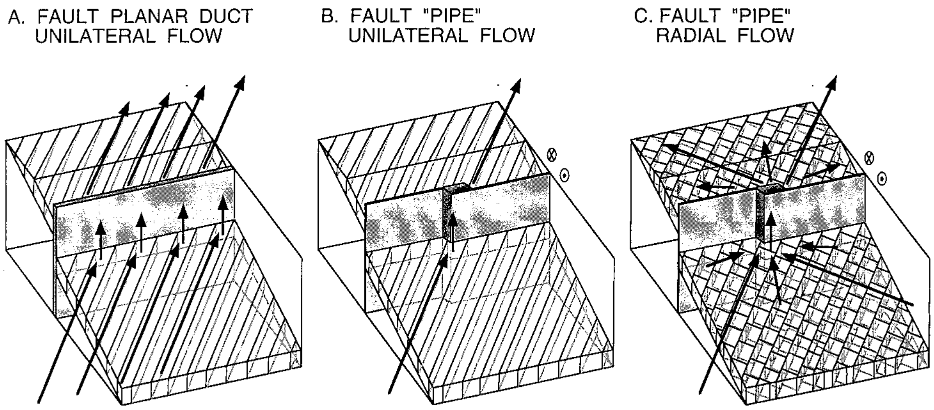

Figure 11. Control of fault structure and source bed permeability anisotropy on basinal fluid-flow geometry in fractured reservoirs. Fluid is depicted to flow updip within fractured source unit into conductive fault and leaves the fault into a fractured reservoir unit at a structurally higher level. A: Fault is uniformly conductive along strike; single fracture set directs fluid flow in single direction. Fault is highly effective in draining the source bed. B: Same as A, but fault is conductive only within stepover region. Fault is poorly effective in draining the source bed. C: Fault is conductive only within stepover region, but two sets of fractures in source and reservoir units allow radial flow pattern into and out of the fault fluid conduit. Fault is highly effective in draining source bed. Fluid flow in Monterey faults is inferred to follow case C. Radial flow in the Monterey Formation may be accommodated by multiple fracture sets or by bedding-parallel brecciation.

ization of cementation and ore mineralization in any crustal environment.

CONCLUSION

Reservoir-scale faults in the Monterey Formation contain locally large volumes of carbonate and minor quartz cement, indicative of large volumes of fluid migrating along these faults. Using the strontium isotopic composition of carbonate cement as a natural tracer for fluid flow, the inferred distance of upward cross-stratigraphic flow approaches the thickness of the Monterey Formation at Jalama Beach of 700 m and appears to constitute a significant fraction of the underlying part of the Monterey Formation at Arroyo Burro Beach. At both locations, the inferred distances suggest that fluid is derived from within the Monterey Formation rather than from underlying older units. Mass-balance estimates of the volume of fluid required for fault cementation at Jalama Beach indicate a minimum distance of formation-parallel flow into the fault zone of 4 to >12 km. Fluid flow is thus highly focused toward this fault zone, the inferred distance of flow parallel to the formation into the fault exceeding the distance of cross-formational upward flow along this fault by at least a factor of six. The mass-balance estimates also suggest that fluid flow along the fault is localized to pipe-shaped channels of limited extent along fault strike, such as releasing bends or stepover regions of overlapping fault segments. Outcrop observations indicate that likely conduits for fluid flow along bedding are layer-confined sets of extension fractures and bedding-parallel breccia bodies, leading to a permeability anisotropy that is intrinsic to the formation rather than controlled by formation boundaries. Fluid flow parallel to bedding into the fault is inferred to follow a radial rather than uni- or bilateral flow symmetry. The inferred radial flow geometry toward fault channels or pipes requires that the permeability structure for flow parallel to bedding is fairly isotropic, whereas flow across bedding is restricted. The isotropic permeability of bedding planes is likely to be caused by multiple sets of extension fractures at high angles to bedding and by bedding-parallel brecciation. The inferred flow geometry illustrates the combined effect of fault permeability structure, permeability anisotropy of the surrounding formation, and hydraulic head distribution in controlling basinal fluid flow in faulted sequences.

ACKNOWLEDGMENTS

This study benefited from discussions with Jim Mattinson, George Tilton, Dave Parkinson, Julie Bryce, Rick Behl, Jon Schwalbach, Rick Sibson, Atilla Aydin, and Rob Knipe. An earlier version of this manuscript was reviewed by Art Sylvester. GSA Associate Editor Elizabeth Burton and reviewers Alden Carpenter and Isabel Montanez provided detailed suggestions for clarification. This project was funded in part by National Science Foundation grant EAR-93-04581 and a grant from the Geological Society of America.

REFERENCES CITED

Barron, J.A., 1986, Updated diatom biostratigraphy for the Monterey Formation of California, *in* Casey, R.E., and Barron, J.A., eds., Siliceous microfossil and microplankton studies of the Monterey Formation and modern analogs: Pacific Section, Society of Economic Paleontologists and Mineralogists Special Publication 45, p. 105–119.

Bartlett, W.L., 1994, Field guide to the Monterey Formation at Ellwood Beach, Santa Barbara County, California, *in* Hornafius, S.J., ed., Field guide to the Monterey Formation between Santa Barbara and Gaviota, California: Pacific Section, American Association of Petroleum Geologists Guide Book, v. 72, p. 95–106.

Baskin, D.K., and Peters, K.E., 1992, Early generation characteristics of a sulfur-rich Monterey kerogen: American Association of Petroleum Geologists Bulletin, v. 76, p. 1–13.

Behl, R.J., and Garrison, R.E., 1994, The origin of chert in the Monterey Formation of California (USA), *in* Iijima, A., ed., Proceedings of the 29th International Geological Congress, Part C, p. 101–132.

Belfield, W.C., Helwig, J., La Pointe, P., and Dahleen, W.K., 1983, South Ellwood Oil Field, Santa Barbara Channel, California, a Monterey Formation fractured reservoir, *in* Isaacs, C.M., and Garrison, R.E., eds., Petroleum generation and occurrence in the Miocene Monterey Formation, California: Los Angeles, Pacific Section, Society of Economic Paleontologists and Mineralogists, p. 213–221.

Boles, J.R., and Ramseyer, K., 1987, Diagenetic carbonate in Miocene sandstone reservoir, San Joaquin Basin, California: American Association of Petroleum Geologists Bulletin, v. 71, p. 1475–1487.

Burns, S.J., and Baker, P.A., 1987, A geochemical study of dolomite in the Monterey Formation, California: Journal of Sedimentary Petrology, v. 57, p. 128–139.

Burns, S.J., Baker, P.A., and Showers, W.J., 1988, The factors controlling the formation and chemistry of dolomite in organic-rich sediments: Miocene Drakes Bay Formation, California, *in* Shukla, V., and Baker, P.A., eds., Sedimentology and geochemistry of dolostones: Society of Economic Paleontologists and Mineralogists Special Publication 43, p. 41–52.

Cande, S.C., and Kent, D.V., 1995, Revised calibration of the geomagnetic polarity timescale for the Late Cretaceous and Cenozoic: Journal of Geophysical Research, v. 100, p. 6093–6095.

Chaudhuri, S., and Clauer, N., 1993, Strontium isotopic compositions and potassium and rubidium contents of formation waters in sedimentary basins: Clues to the origin of the solutes: Geochimica et Cosmochimica Acta, v. 57, p. 429–437.

Compton, J.S., 1988, Sediment composition and precipitation of dolomite and pyrite in the Neogene Monterey and Sisquoc Formations, Santa Maria Basin area, California, *in* Shukla, V., and Baker, P.A., eds., Sedimentology and geochemistry of dolostones: Society of Economic Paleontologists and Mineralogists Special Publication 43, p. 53–64.

Compton, J.S., 1991, Origin and diagenesis of clay minerals in the Monterey Formation, Santa Maria Basin area, California: Clay and Clay Minerals, v. 39, p. 449–466.

Crain, W.E., Mero, W.E., and Patterson, D., 1985, Geology of the Point Arguello discovery: American Association of Petroleum Geologists Bulletin, v. 69, p. 537–545.

DePaolo, D.J., and Finger, K.L., 1991, High-resolution strontium-isotope stratigraphy and biostratigraphy of the Miocene Monterey Formation, central California: Geological Society of America Bulletin, v. 103, p. 112–124.

Dholakia, S.K., Aydin, A., Pollard, D.D., and Zoback, M.D., 1998, Development of fault-controlled hydrocarbon migration pathways in the Monterey Formation, California: American Association of Petroleum Geologists Bulletin, v. 82, p. 1551–1574.

Dibblee, T.W., Jr., 1988a, Geologic map of the Lompoc Hills and Point Conception Quadrangles, Santa Barbara County, California: Santa Barbara, California, Dibblee Foundation, scale 1:24 000.

Dibblee, T.W., Jr., 1988b, Geologic map of the Tranquillon Mtn. and Point Arguello Quadrangles, Santa Barbara County, California: Santa Barbara, California, Dibblee Foundation, scale 1:24 000.

Echols, R.J., 1994, Biostratigraphy of the Luisian and Mohnian Stages between Santa Barbara and Gaviota, California, *in* Hornafius, S.J., ed., Field guide to the Monterey Formation between Santa Barbara and Gaviota, California: Pacific Section, American Association of Petroleum Geologists Guide Book, v. 72, p. 29–44.

Eichhubl, P., 1997, Scale, rates, and timing of fracture-related fluid flow in the Miocene Monterey Formation, Coastal California [Ph.D. dissert.]: Santa Barbara, University of California, 298 p.

Eichhubl, P., and Behl, R.J., 1998, Field guide to ''Diagenesis, deformation, and fluid flow in the Miocene Monterey Formation'': Ventura–Santa Barbara–Jalama Beach–Grefco Quarry/Lompoc, *in* Eichhubl, P., ed., Diagenesis, deformation, and fluid flow in the Miocene Monterey Formation: Pacific Section, SEPM (Society for Sedimentary Geology) Special Publication 83, p. 85–98.

Eichhubl, P., and Boles, J.R., 1998, Vein formation in relation to burial diagenesis in the Miocene Monterey Formation, Arroyo Burro Beach, Santa Barbara, California, *in* Eichhubl, P., ed., Diagenesis, deformation, and fluid flow in the Miocene Monterey Formation: Pacific Section, SEPM (Society for Sedimentary Geology) Special Publication 83, p. 15–36.

Ellis, A.J., 1959, The solubility of calcite in carbon dioxide solutions: American Journal of Science, v. 257, p. 354–365.

Ellis, A.J., and Golding, R.M., 1963, The solubility of carbon dioxide above 100°C in water and in sodium chloride solutions: American Journal of Science, v. 261, p. 47–60.

Faure, G., 1986, Principles of isotope geology (second edition): New York, Wiley, 589 p.

Feldman, M.D., Kwon, S.-T., Boles, J.R., and Tilton, G.R., 1993, Diagenetic mass transport in the southern San Joaquin basin, California, U.S.A.: Implications from the strontium isotopic composition of modern pore fluids: Chemical Geology, v. 110, p. 329–343.

Grivetti, M.C., 1982, Aspects of stratigraphy, diagenesis, and deformation in the Monterey Formation near Santa Maria–Lompoc, California [Master's thesis]: Santa Barbara, University of California, 155 p.

Gross, M.R., 1993, The origin and spacing of cross-joints: Examples from the Monterey Formation, Santa Barbara coastline, California: Journal of Structural Geology, v. 15, p. 737–751.

Gross, M.R., 1995, Fracture partitioning: Failure mode as a function of lithology in the Monterey Formation of coastal California: Geological Society of America Bulletin, v. 107, p. 779–792.

Gross, M.R., Gutiérrez-Alonso, G., and Bartlett, W.L., 1998, Fold-related fractures in coastal outcrops of the Monterey Formation: Effects on structural style, mechanical stratigraphy, and scale at Arroyo Burro Beach, *in* Eichhubl, P., ed., Diagenesis, deformation, and fluid flow in the Miocene Monterey Formation: Pacific Section, SEPM (Society for Sedimentary Geology) Special Publication 83, p. 37–65.

Hickman, R.G., and Dunham, J.B., 1992, Controls on the development of fractured reservoirs in the Monterey Formation of central California, *in* Larsen, R.M., et al., eds., Structural and tectonic modeling and its application to petroleum geology: Amsterdam, Elsevier, p. 343–353.

Hill, D.P., 1977, A model for earthquake swarms: Journal of Geophysical Research, v. 82, p. 347–352.

Hornafius, S.J., 1994a, Overview of the stratigraphy of the Monterey Formation along the coastline between Santa Barbara and Gaviota, California, *in* Hornafius, S.J., ed., Field guide to the Monterey Formation between Santa Barbara and Gaviota, California: Pacific Section American Association of Petroleum Geologists Guide Book, v. 72, p. 1–15.

Hornafius, S.J., 1994b, Correlation of volcanic ashes in the Monterey Formation between Naples Beach and Gaviota Beach, California, *in* Hornafius, S.J., ed., Field guide to the Monterey Formation between Santa Barbara and Gaviota, California: Pacific Section, American Association of Petroleum Geologists Guide Book, v. 72, p. 45–58.

Hornafius, S.J., 1994c, Field trip log to the Monterey Formation between Santa Barbara and Gaviota, California, *in* Hornafius, S.J., ed., Field guide to the Monterey Formation between Santa Barbara and Gaviota, California: Pacific Section, American Association of Petroleum Geologists Guide Book, v. 72, p. 107–123.

Howarth, R.J., and McArthur, J.M., 1997, Statistics for strontium isotope stratigraphy: A robust LOWESS fit to the marine Sr-isotope curve for 0 to 206 Ma, with look-up table for derivation of numeric age: Journal of Geology, v. 105, p. 441–456.

Isaacs, C.M., 1980, Diagenesis in the Monterey Formation examined laterally along the coast near Santa Barbara, California [Ph.D. dissert.]: Stanford, California, Stanford University, 329 p.

Isaacs, C.M., 1981, Outline of diagenesis in the Monterey Formation examined laterally along the Santa Barbara coast, California, *in* Isaacs, C.M., ed., Guide to the Monterey Formation in the California coastal area, Ventura to San Luis Obispo: Pacific Section, American Association of Petroleum Geologists, v. 15, p. 25–38.

Isaacs, C.M., and Petersen, N.F., 1987, Petroleum in the Miocene Monterey Formation, California, *in* Hein, J.R., ed., Siliceous sedimentary rock-hosted ores and petroleum: New York, Van Nostrand Reinhold, p. 83–116.

Jackson, P.A., and Yeats, R.S., 1982, Structural evolution of Carpinteria Basin, Western Transverse Ranges, California: American Association of Petroleum Geologists Bulletin, v. 66, p. 805–829.

Lundegard, P.D., and Land, L.S., 1989, Carbonate equilibria and pH buffering by organic acids—Response to changes in p_{CO_2}: Chemical Geology, v. 74, p. 277–287.

MacKinnon, T.C., 1989, Petroleum geology of the Monterey Formation in the Santa Maria and Santa Barbara coastal and offshore areas, *in* MacKinnon, T.C., ed., Oil in the California Monterey Formation: American Geophysical Union, Field Trip Guide Book T311, p. 11–27.

Malone, M.J., Baker, P.A., and Burns, S.J., 1994, Recrystallization of dolomite: Evidence from the Monterey Formation (Miocene), California: Sedimentology, v. 41, p. 1223–1239.

Miller, N.R., 1995, Lithostratigraphic signal evaluation of the Miocene Monterey Formation, South Elwood Field, Santa Barbara–Ventura Basin, California [Ph.D. dissert.]: Dallas, Texas, University of Dallas, 606 p.

Mountjoy, E.W., Qing, H., and McNutt, R.H., 1992, Strontium isotopic composition of Devonian dolomites, Western Canada sedimentary basin: Significance of sources of dolomitizing fluids: Applied Geochemistry, v. 7, p. 59–75.

Narr, W., 1991, Fracture density in the deep subsurface: Techniques with application to Point Arguello Oil Field: American Association of Petroleum Geologists Bulletin, v. 75, p. 1300–1323.

Ogle, B.A., Wallis, W.S., Heck, R.G., and Edwards, E.B., 1987, Petroleum geology of the Monterey Formation in the offshore Santa Maria/Santa Barbara areas, *in* Ingersoll, R.V., and Ernst, W.G., eds., Cenozoic basin development of coastal California: Englewood Cliffs, New Jersey, Prentice-Hall, p. 382–406.

Petersen, N.F., and Hickey, P.J., 1987, California Plio-Miocene oils; evidence of early generation, *in* Meyer, R.F., ed., Exploration for heavy crude oil and natural bitumen: American Association of Petroleum Geologists Studies in Geology, v. 25, p. 351–359.

Pisciotto, K.A., and Garrison, R.E., 1981, Lithofacies and depositional environments of the Monterey Formation, California, *in* Garrison, R.E., and Douglas, R.G., eds., The Monterey Formation and related siliceous rocks of California: Pacific Section, Society of Economic Paleontologists and Mineralogists Special Publication. 15, p. 97–122.

Pollastro, R.M., 1990, Geothermometry from smectite and silica diagenesis in the diatomaceous Monterey and Sisquoc Formations, Santa Maria Basin, California: American Association of Petroleum Geologists Bulletin, v. 74, p. 742.

Redwine, L.E., 1981, Hypothesis combining dilation, natural hydraulic fracturing, and dolomitization to explain petroleum reservoirs in Monterey Shale, Santa Maria area, California, *in* Garrison, R.E., and Douglas, R.G., eds., The Monterey Formation and related siliceous rocks of California: Pacific Section, Society of Economic Paleontologists and Mineralogists Special Publication 15, p. 221–248.

Roehl, P.O., 1981, Dilation brecciation—A proposed mechanism of fracturing, petroleum expulsion and dolomitization in the Monterey Formation, California, *in* Garrison, R.E., and Douglas, R.G., eds., The Monterey Formation and related siliceous rocks of California: Pacific Section, Society of Economic Paleontologists and Mineralogists Special Publication 15, p. 285–315.

Roehl, P.O., and Weinbrandt, R.M., 1985, Geology and production characteristics of fractured reservoirs in the Miocene Monterey Formation, West Cat Canyon Oilfield, Santa Maria Valley, California, *in* Roehl, P.O., and Choquette, P.W., eds., Carbonate petroleum reservoirs: New York, Springer, p. 526–545.

Schultz, J.L., Boles, J.R., and Tilton, G.R., 1989, Tracking calcium in the San Joaquin basin, California: A strontium isotopic study of carbonate cements at North Coles Levee: Geochimica et Cosmochimica Acta, v. 53, p. 1991–1999.

Shackleton, N.G., Crowhurst, S., Hagelburg, T., Pisias, N., and Schneider, D., 1994, A new late Neogene time scale: Application to Leg 138 Sites, *in* Proceedings of the Ocean Drilling Program, Scientific results, Volume 138: College Station, Texas, Ocean Drilling Program, p. 73–101.

Sibson, R.H., 1996, Structural permeability of fluid-driven fault-fracture meshes: Journal of Structural Geology, v. 18, p. 1031–1042.

Smith, J.T., and Ehrenberg, S.N., 1989, Correlation of carbon dioxide abundance with temperature in clastic hydrocarbon reservoirs: Relationship to inorganic chemical equilibrium: Marine and Petroleum Geology, v. 6, p. 129–135.

Snyder, W.S., Brueckner, H.K., and Schweickert, R.A., 1983, Deformational styles in the Monterey Formation and other siliceous sedimentary rocks, *in* Isaacs, C.M., and Garrison, R.E., eds., Petroleum generation and occurrence in the Miocene Monterey Formation, California: Los Angeles, Pacific Section, Society of Economic Paleontologists and Mineralogists, p. 151–170.

Stein, C.L., and Kirkpatrick, R.J., 1976, Experimental porcelanite recrystallization kinetics: A nucleation and growth model: Journal of Sedimentary Petrology, v. 46, p. 430–435.

Sullivan, M.D., Haszeldine, R.S., and Fallick, A.E., 1990, Linear coupling of carbon and strontium isotopes in Rotliegend Sandstone, North Sea: Evidence for cross-formational fluid flow: Geology, v. 18, p. 1215–1218.

Ungerer, P., Behar, E., and Discamps, D., 1983, Tentative calculation of the overall volume expansion of organic matter during hydrocarbon genesis from geochemistry data. Implications for primary migration: Proceedings of the International Meeting on Organic Geochemistry (Advances in Organic Geochemistry 1981), v. 10, p. 129–135.

U.S. Geological Survey, 1983, Geology and reservoir characteristics of the Santa Ynez Unit, Santa Barbara Channel, off California, *in* Isaacs, C.M., and Garrison, C.M., eds., Petroleum generation and occurrence in the Miocene Monterey Formation, California: Los Angeles, Pacific Section, Society of Economic Paleontologists and Mineralogists, p. 111–130.

Manuscript Received by the Society August 20, 1998
Revised Manuscript Received July 22, 1999
Manuscript Accepted November 18, 1999

Printed in the USA